### Title
Observation of an Orientational Glass in a Superlattice of Elliptically-Faceted CdSe Nanocrystals




### Journal
ACS Nano, 16(6)

### ISSN
1936-0851



### Authors
Abbas, Abdullah S
Vargo, Emma
Jamali, Vida
et al.



### Publication Date
2022-06-28

### DOI
10.1021/acsnano.2c02014

Peer reviewed

# Observation of an Orientational Glass in a Superlattice of Elliptically-Faceted CdSe Nanocrystals

*Abdullah S. Abbas[1], Emma Vargo[1], Vida Jamali[2], Peter Ercius[4], Priscilla F. Pieters[2], Rafaela M. Brinn[2], Assaf Ben-Moshe[2,3], Min Gee Cho[4], Ting Xu[1,2,3], A. Paul Alivisatos[1,2,3,5,†*]*

[1]Department of Materials Science and Engineering, University of California, Berkeley, California 94720, United States

[2]Department of Chemistry, University of California, Berkeley, California 94720, United States

[3]Materials Sciences Division, Lawrence Berkeley National Laboratory, Berkeley, California 94720, United States

[4]National Center for Electron Microscopy, Molecular Foundry, Lawrence Berkeley National Laboratory, Berkeley, CA 94720, USA.

[5]Kavli Energy NanoScience Institute, Berkeley, California 94720, United States

[†]Present address: Department of Chemistry and Pritzker School of Molecular Engineering, University of Chicago, Chicago, Illinois 60637, United States

*To whom correspondence may be addressed: paul.alivisatos@berkeley.edu

ABSTRACT

Extensive prior work has shown that colloidal inorganic nanocrystals coated with organic ligand shells can behave as artificial atoms and, as such, form superlattices with different crystal structures and packing densities. Although ordered superlattices present a high degree of long-range positional order, the relative crystallographic orientation of the inorganic nanocrystals with respect to each other tends to be random. Recent works have shown that superlattices can achieve orientational alignment through combinations of nanocrystal faceting and ligand modification, as well as selective metal particle attachment to particular facets. These studies have focused on the assembly of high-symmetry nanocrystals, such as cubes and cuboctahedra. Here, we study the assembly of elliptically-faceted CdSe/CdS core/shell nanocrystals with one unique crystallographic orientation along the major elliptical axis. We show that the nanocrystals form an unexpectedly well-ordered translational superlattice, with a degree of order comparable to that achieved with higher-symmetry nanocrystals. Additionally, we show that, due to the particles' faceted shape, the superlattice is characterized by an orientational glass phase in which only certain orientations are possible due to entropically-frustrated crystallization. In this phase, the nanocrystals do not exhibit a local orientational ordering but rather have distinct orientations that emerge at different locations within the same domain. The distinct orientations are a result of a facet-to-facet lock-in mechanism that occurs during the self-assembly process. These facet-to-facet alignments force the nanocrystals to tilt on different lattice planes forming different projections that we termed apparent polydispersity. Our experimental realization of an orientational glass phase for multifaceted semiconducting nanocrystals will allow further

investigation of how this phase is formed and how it can be utilized for potential optical, electrical, and thermal transport applications.

KEYWORDS: Nanocrystals, Self-Assembled Superlattice, Cadmium Chalcogenide, Autocorrelation, Orientational Glass.

The self-assembly of colloidal inorganic nanocrystals into 2D and 3D superlattices has drawn significant attention in the field of functional nanomaterials[1–3]. Different techniques and mechanisms have been developed for nanocrystal self-assembly[4]; notably, self-assembly of nanocrystals at liquid-air interfaces has proven to be a reliable technique for forming well-ordered superlattices with high packing densities[4]. One of the structures commonly formed by these assemblies is a hexagonal superlattice, with either FCC-on (111) or HCP-on (0001) packing[4]. When discussing ordering in superlattices, one must consider not only translational order, but also the orientational order of the crystallographic axes between nanocrystals. Self-assembled nanocrystal superlattices generally possess high translational order and are often superior in this regard to epitaxially-prepared superlattices[5]. Yet, computer simulations demonstrate that the nanocrystals' shape plays a major role in determining whether they can form a single crystal, as their density increases, or become a disordered superlattice[6–8]. In between these two phases, liquid crystals and plastic crystals can also form based on the shape of the nanocrystals. Liquid crystals have high orientational order but lack long-range translational order, while plastic crystals have high translational order but lack long-range orientational order. One type of plastic crystal phase is the orientational glass phase, which can form from multi-faceted nanocrystals with polyhedral shapes[8]. The orientational glass phase occurs when the nanocrystals form translationally-ordered superlattices with a limited set of preferred crystallographic orientations. The orientation of individual nanocrystals can match each other at different locations within the same domain. Figure 1 compares a single crystal with perfect translational and orientational order and a plastic crystal with perfect translational order but no orientational order to an orientational glass phase with a high degree of translational order, but a limited set of preferred crystallographic orientations. While the formation of orientational glass

phases has been shown in computer simulation for nanocrystal superlattices, to our knowledge, it has not been documented or discussed in previous experimental works on nanocrystal superlattices[9,10].

Recently, significant developments in orientationally-ordered high-symmetry nanocrystals (quasi-spherical, cube-shaped, cuboctahedral, and others) within superlattices have been reported[11–14]. Efforts have been focused on modulating surface ligands, including varying the ligand length or ligand coverage, in order to accentuate the effects of the underlying inorganic nanocrystal facets[12,15]. Although it is possible to exchange the long ligands with shorter ones to increase nanocrystal-to-nanocrystal coupling, this approach requires harsh post-processing that often introduces disorder in the orientational alignment within the superlattice[16]. An alternative approach for achieving orientational alignment is modifying the nanocrystal facets by attaching metal nanoparticles, so the stronger van der Waals interactions between the metal nanoparticles can be exploited to guide the alignment of the underlying nanocrystals[9]. Although adding metal nanoparticles to the nanocrystals results in orientational alignment, the metal nanoparticles are far from neutral and, among other effects, they may quench the semiconductor nanocrystal luminescence.

In this work, we investigate the assembly of lower-symmetry, elliptically-faceted wurtzite CdSe/CdS core/shell nanocrystal superlattices, and we report the formation of the so-called orientational glass phase. Although highly-monodisperse nanocrystals are normally needed to form a highly-ordered superlattice, we find that the formation of an orientational glass phase relies on the geometry of the nanocrystals rather than the monodispersity of the ensemble (figure S1). In the orientational glass phase, due to the elliptically-faceted shape, the nanocrystals take

on different tilts resulting in different shapes from a 2D projection, including faceted ellipsoids, spheres, and hexagons, as shown in figure S2. The various tilts of the nanocrystals result in an apparent polydispersity, which acts as a point defect and weakens the translational order of the superlattice. This work provides a better understanding of orientational ordering in self-assembling semiconductor nanocrystals and can be used to fabricate new types of 2D and 3D functional nanomaterials.

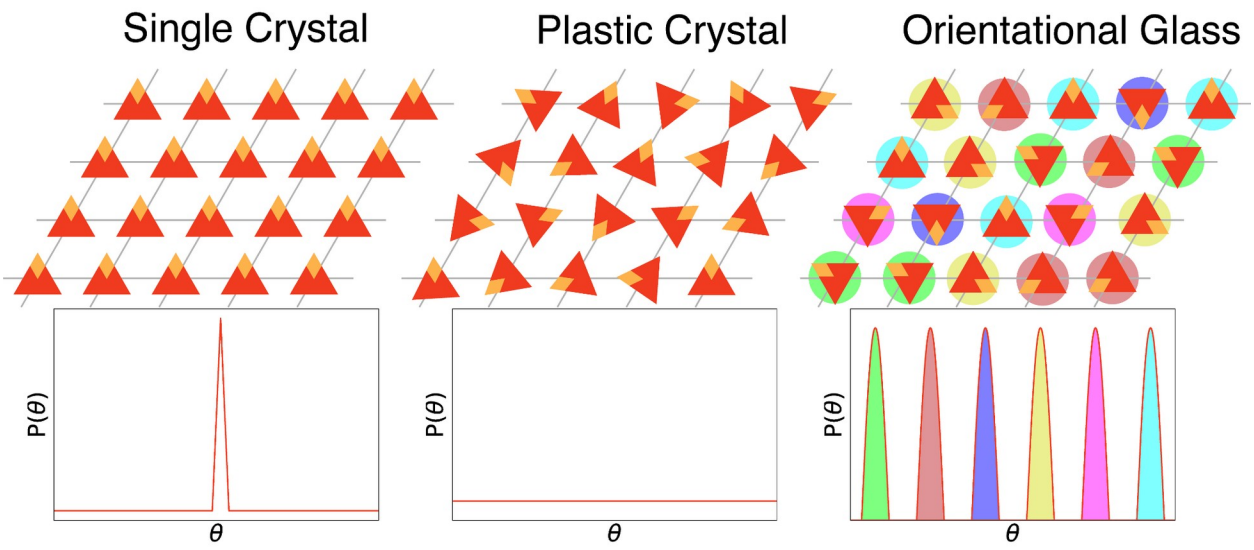


**Figure 1.** 2D hexagonal lattice and orientational probability, P(□), for different phases: Single crystal with perfect translational and orientational order, plastic crystal with good translational order and no orientational order, and orientational glass with good translational order and only certain allowed orientations. The particles are color-coded to show the distinct orientations and the possibility of short-range orientational correlation.

RESULTS AND DISCUSSION

**Isotropic vs Anisotropic Nanocrystals.**

Kinetic studies of nanocrystal self-assembly reveal that neighboring nanocrystals tend to orient early in the assembly process[17]. This suggests that the shape of nanocrystals and a facet-to-facet lock-in mechanism ought to eventually result in crystallographic alignment of the nanocrystals in the superlattice, as this maximizes packing at high densities[17]. To investigate the effect of the nanocrystal shape on the crystallographic alignment and order, we prepared wurtzite CdSe/CdS core/shell nanocrystals capped with oleic acid and oleylamine ligands with two shapes. The two shapes are: quasi-spherical nanocrystals in which the facets are small and smoothened by the ligands (figure S3), and elliptically-faceted nanocrystals that are more elongated in shape such that the facets are prominent even with ligands coverage (figure S4).

The transmission electron microscopy (TEM) image and the small-angle Selected Area Electron Diffraction (SAED) pattern in figure 2a-b show a translationally well-ordered superlattice consisting of quasi-spherical nanocrystals. Despite the translational order in the quasi-spherical nanocrystal superlattice (figure 2b), the wide-angle SAED pattern in figure 2c with isotropic rings clearly indicates that the individual nanocrystals within the superlattices are randomly oriented. This is in agreement with previous observations by Zhu *et al.* showing random orientations for undecorated quasi-spherical nanocrystals[9]. Figure 2d-e show that for slightly elliptical and faceted nanocrystals, however, the self-assembled superlattices maintain high translational order, while also displaying a set of preferred orientations. These orientations appear as anisotropic rings in the diffraction pattern of figure 2f. There are azimuthal peaks characterized by an average full width at half maximum angle of 20-30$^{o}$ (figure S5). This level of peak broadening is consistent with previous observations of partial orientational order in both

Au-decorated CdSe and truncated octahedron PbS systems as well as the $CBr_4$ molecular system[9,12,17–19].

Our wurtzite CdSe/CdS core/shell nanocrystals are characterized by an elongated hexagonal bipyramidal shape that is truncated along the (0002) plane, resembling a faceted ellipsoid with an average aspect ratio of 1.2 (more details in figure S6), which is similar to a previously observed nanocrystal shape[20]. The nanocrystals show distinct facets, as modelled in figure 2g-h and experimentally verified using High-Angle Annular Dark-Field Scanning Transmission Electron Microscopy (HAADF-STEM) and its corresponding Fast Fourier Transform (FFT) in figure 2i-j (and figure S4). This model is in agreement with a previously-published result on CdSe/CdS core/shell nanocrystals[21]. Previous work on PbS nanocrystals has shown that ligand to ligand interactions have a strong influence on orientational alignments[12,22]. Thus, to ensure that the facets are responsible for the observed orientational alignment in this study, we performed several aggressive washes of the nanocrystals to remove as many ligands as possible and performed NMR to qualitatively confirm the reduction of the ligand coverage on the nanocrystal surfaces and removal of unbound ligands. Based on the NMR results in figure S7, we found that the ligand density does not have a significant effect on the orientational alignment of nanocrystals within the superlattices.

The interesting phase observed in figure 2d-f is characterized by translational order and a set of limited and distinct crystallographic orientations for nanocrystals within a superlattice. The close resemblance to simulations in the literature suggest that this may be an orientational glass. An orientational glass phase arises when nanocrystals are entropically locked into distinct local orientations with respect to neighboring nanocrystals during the self-assembly process. In this

case, an orientationally-ordered crystalline phase is not inherently more favorable, since many orientations of nanocrystals would result in the same entropy for the system[23,24]. The orientational glass phase was reported in simulations by Glotzer and coworkers for pseudorhom-bicuboctahedron hard particles, where nanoparticles adopted a set of only six distinct orientations at high packing density[25].

In order to confirm the formation of an orientational glass phase within our superlattice, we used wide-angle SAED to find the lattice planes of nanocrystals. The first three rings in figure 2c correspond to the $(10\bar{1}0)$, $(10\bar{1}1)$ and $(0002)$ lattice planes in CdSe wurtzite crystal structure. Since we observe crystallographic patterns in all lattice planes in the elliptically-faceted nanocrystals, it is expected that some particles lay flat on the $(10\bar{1}0)$ plane, some tilt on the $(10\bar{1}1)$ plane, while others stand on the $(0002)$ plane. From this variation in out-of-plane tilt angles, the 2D projected shape of individual nanocrystals results in an apparent polydispersity regardless of how monodisperse the constituent nanocrystals are (figure S2). This apparent polydispersity affects the packing of nanocrystals and shows up as relatively weaker translational ordering, as will be described in the following section.

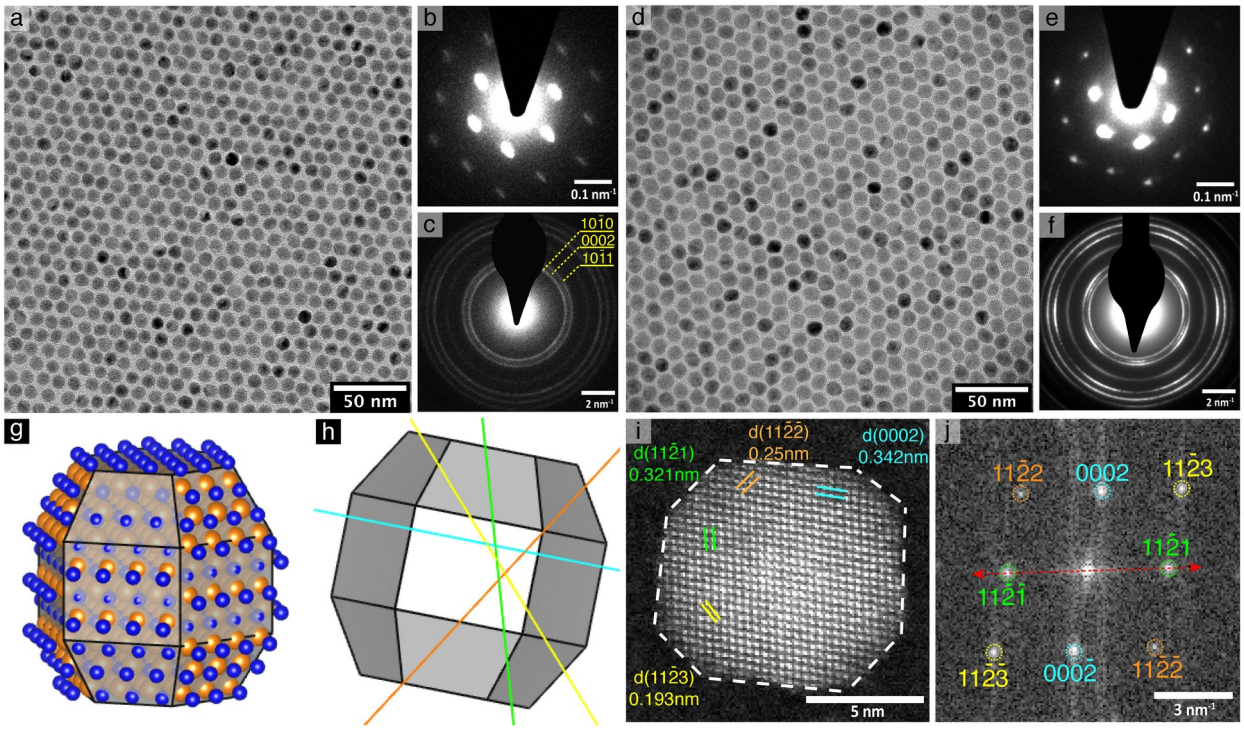


**Figure 2.** (a-c) Quasi-spherical nanocrystals compared to (d-f) oriented elliptically-faceted nanocrystals. (a,d) TEM images of a quasi-spherical nanocrystal monolayer superlattice and a elliptically-faceted nanocrystal monolayer superlattice. (b,e) Small-angle SAED showing positional order in the superlattice. (c,f) Wide-angle Selected Area Electron Diffraction (SAED) showing random vs ordered orientational alignment in the lattice planes of individual wurtzite CdSe/CdS core/shell nanocrystals from quasi-spherical and elliptically-faceted nanocrystals, respectively. The three first rings from the center labelled in (c) correspond to the CdSe wurtzite crystal lattice planes. (g) 3D model of elliptically-faceted nanocrystals with (h) rotated to match the lattice planes labelled with cyan $(0002)$, green $(11\acute{2}1)$, yellow $(11\acute{2}3)$, and orange $(11\acute{2}2)$ lines on (i,j) HAADF-STEM and Fast Fourier Transform (FFT).

**Translational Order.**

The translational order of the elliptically-faceted and oriented nanocrystal superlattices can be seen in figure 3. The analysis closely follows the work of Pichler *et al.* where an autocorrelation function, $ACF(r)$, is used to analyze the distance, r, over which particles influence each other's position in a self-assembled superlattice[5]. Correlation along a relatively large r suggests a crystal structure with long-range translational order. The ACF has the form:

$$ACF_{fit}(r) = A_\infty + f_0 e^{\text{¿¿}} \quad (1)$$

The first term, $A_\infty$ is the asymptotic level that the peak envelope converges to at infinity[5]. The second term is a Gaussian function that accounts for point defects, resulting from size and shape polydispersity, and vacancies, and the third term is an additional Gaussian function that accounts for lattice distortions[5]. $f_0$ and $\sigma_0$, along with $f$ and $\sigma$ are the first and second Gaussian amplitudes and widths, respectively[5]. After fitting the ACF(r), the long-range order $\xi_{lr}$ (equation 2), short range order $\kappa_{sr}$ (equation 3) and the degree of anisotropy in ordering $a$ (equation 4) parameters are then extracted as follows[5]:

$$\xi_{lr} = \frac{A_\infty}{(f + A_\infty)} \quad (2)$$

$$\kappa_{sr} = \sigma \frac{(f + A_\infty)}{f} \quad (3)$$

$$a = \sqrt{\frac{1}{n}\sum_{i}^{n} \left(acv_i - ACF_{fit}(r_i)\right)^2} \quad (4)$$

In Eq. (4), the subscripts i corresponds to the data points incrementally, namely for each peak in the oscillation along a direction, while n is the total data points along the direction analyzed. Figure 3a is a result of running a 2D autocorrelation function on figure 2d. The directions were then selected from the center of the image indicated in red, and they follow the underlying lattice. Figure 3b shows a rapid drop in the translational autocorrelation function ACF(r), which

is typically attributed to point defects in the superlattice. Yet, the Delaunay triangulation and the Voronoi diagram in figure 3d-e show that the majority of the cells are uniform indicating that the superlattice is formed with minimal defects and vacancies[26,27]. Thus, we instead attribute the rapid drop to the fact that our nanocrystals have an apparent polydispersity: 2D projections of nanocrystals with different orientations present different shapes, including faceted ellipsoids, spheres, and hexagons resulting in a broad distribution of diameters (figure 3f) and a non-uniform center-to-center spacing (figure 3g) between the nanocrystals. With this apparent polydispersity, the lattice distortion is more significant than that observed in isotropic nanocrystals by Pichler *et al.*, resulting in a weak long-range ordering in our system but with a good degree of short-range ordering[5]. Moreover, the differences in the decay of the autocorrelation function curves in different directions as shown in figure 3a,b is expected and can be attributed to the anisotropic nature of our nanocrystals in which their apparent polydispersity and their varying interparticle spacings are direction-dependent. In each direction, the nanocrystals can have different orientations. This variation in local orientations and interparticle spacing causes a different amount of shift in nanocrystals' positional alignment for different directions causing the discrepancy among the three directions.

Figure 3c illustrates the values for the long range and short-range order as well as anisotropy for the three directions shown in figure 3a (larger area analysis shown in figure S8). For a perfectly-ordered crystal with long-range translational order, $\xi_{lr} \to 1$ and $\kappa_{sr} \to \infty$ , while in the absence of any long-range order, $\xi_{lr}$ approaches zero and $\kappa_{sr}$ equals $\sigma$. Overall, our nanocrystals formed a superlattice with a surprisingly high degree of translational order.

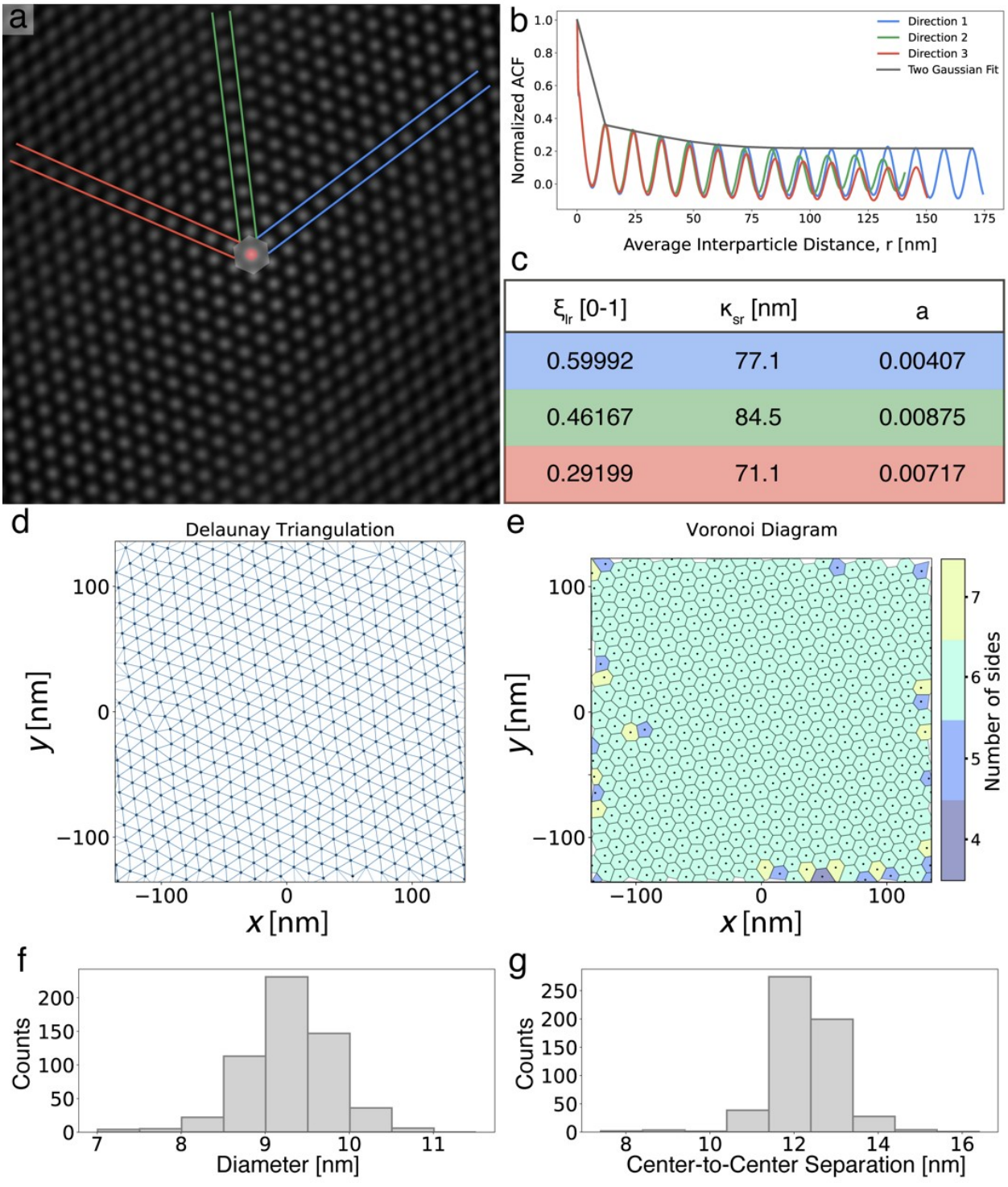


| $\xi_{lr}$ [0-1] | $\kappa_{sr}$ [nm] | a |
|---|---|---|
| 0.59992 | 77.1 | 0.00407 |
| 0.46167 | 84.5 | 0.00875 |
| 0.29199 | 71.1 | 0.00717 |

**Figure 3.** Translational order in the faceted elliptical nanocrystal superlattice. (a) Translational 2D autocorrelation function map of the elliptically-faceted nanocrystal superlattice TEM image

in figure 2d, with three major directions (indicated in blue, green, and red) plotted in (b) to show the translational order in the superlattice. (c) Fitted parameters of the autocorrelation function in (b) (black curve) showing long-range and short-range order, along with the anisotropy parameters that are extracted based on the two Gaussian fits. (d) Delaunay Triangulation mapping the center of mass of the elliptically-faceted nanocrystals in the superlattice to show nanocrystal separations. (e) Voronoi Diagram showing the expected six-fold symmetry in the hexagonal superlattice with minimal point defects. (f-g) Histograms indicate a relatively wide distribution both in apparent nanocrystal size and center-to-center separation.

**Orientational Order.**

Previous work suggests that during self-assembly, the elliptically-faceted nanocrystals likely lose some rotational degrees of freedom due to facet-to-facet lock-in alignment that occurs early in the assembly process[17,28]. At higher packing densities, the rotational dynamics slow down and the nanocrystals freeze in a limited set of distinct orientations, consistent with the wide-angle SAED (figure 2f)[25].

From the aberration corrected High Resolution Transmission Electron Microscopy (HRTEM) image in figure 4a, each nanocrystal is analyzed to find at least two lattice planes, as required to identify the zone axis. The d-spacing of each lattice plane and the corresponding orientation is then extracted (see methods). While the orientation of most nanocrystals could be identified, some remain ambiguous due to the low symmetry of the nanocrystal orientation with respect to the beam direction. From the d-spacing and the orientations of lattice planes for nanocrystals in

the selected region in figure 4a, we overlaid the crystal model as shown in figure 4b (more examples are shown in figure S4).

Although the ensemble diffraction measurements of our superlattices show distinct orientational alignment, upon careful investigation of our results shown in figure 4a, we were not able to correlate the orientational order in the superlattice as one can do for single crystals. The lattice does not exhibit a grained structure with local orientational ordering and grain boundaries. Instead, we find that a nanocrystal's orientation can differ from its surrounding nanocrystals with only certain possible short-range correlation within 3-fold rotation, but its orientation is still correlated to other nanocrystals within the superlattice, giving rise to the observed distinct orientational alignment in figure 2f. This is the signature of an orientational glass phase.

From the extracted d-spacing and lattice plane orientations, the azimuthal angles corresponding to $(0002)$ and $(10\acute{1}1)$ planes from all identified nanocrystals are plotted in figure 4c where each point indicates the angle of the lattice within the superlattice. The results show a trimodal distribution indicating that the nanocrystals can only have a set of preferred orientations, which is in agreement with the wide-angle SAED patterns in figure 2f.

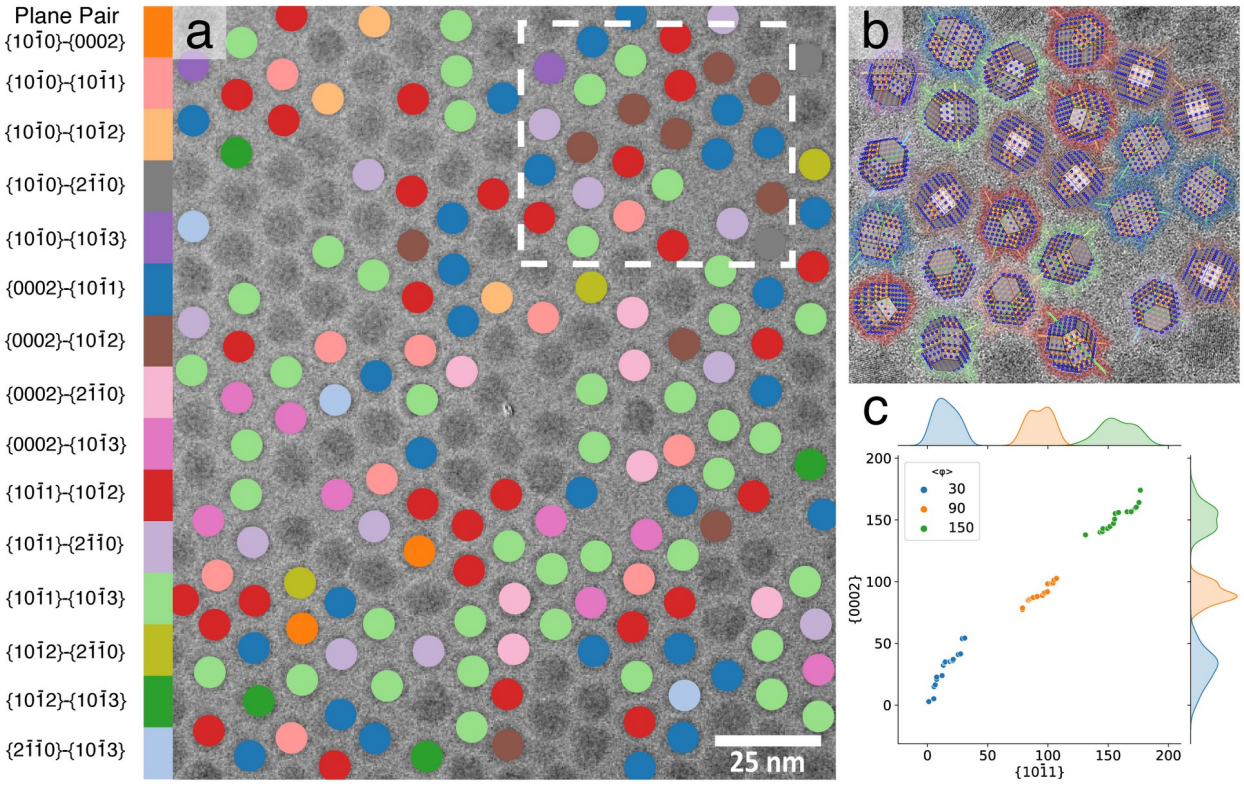


**Figure 4.** Orientational order in the elliptically-faceted nanocrystal superlattice. (a) Aberration corrected HRTEM image of the superlattice with color-coded overlay based on zone axes consisting of two lattice planes, with a key shown on the far left. The map shows only very local orientational correlation with each color emerging at different locations; this is good evidence for the orientational glass phase. (b) selected area from (a) overlaid with the crystal models based on the nanocrystal 3D orientation estimated from the lattice plane orientations, with color shading corresponding to the colors in the selected area. (c) Scatter plot of $(0002)$and $(10\bar{1}1)$ planes where the corresponding azimuthal angle of each lattice plane is extracted from individual nanocrystals, showing a trimodal distribution.

It is interesting that our nanocrystals with apparent polydispersity, including both size and shape, can still form this orientational glass phase, demonstrating that a highly monodisperse system is not necessarily required to achieve an orientational glass phase. The key element is the geometry, which determines how the nanocrystals align. This is evident in the two studied shapes in which quasi-spherical nanocrystals possessed no distinct orientations compared to the elliptically-faceted nanocrystals. The distinct alignments of the nanocrystals in this orientational glass phase may assist in studying carrier and energy transfer. Additionally, the orientational glass phase not only occurs in a 2D monolayer superlattice. We show that similar structures can also form in bilayer, multilayer, or even 3D supercrystals as shown in figure 5 (thickness analysis in figure S9), and we can form superlattices with FCC-on (100) structure in addition to the HCP (0001) structure as seen in figure S10.

Since CdSe/CdS core/shell nanocrystals are a prototypical system for many purposes, it is particularly interesting to experimentally observe the formation of an orientational glass phase for these polyhedral nanocrystals. This work may be useful for the fundamental understanding of how this phase is formed and how it can be utilized for potential optoelectronic, mechanical, and thermal transport applications.

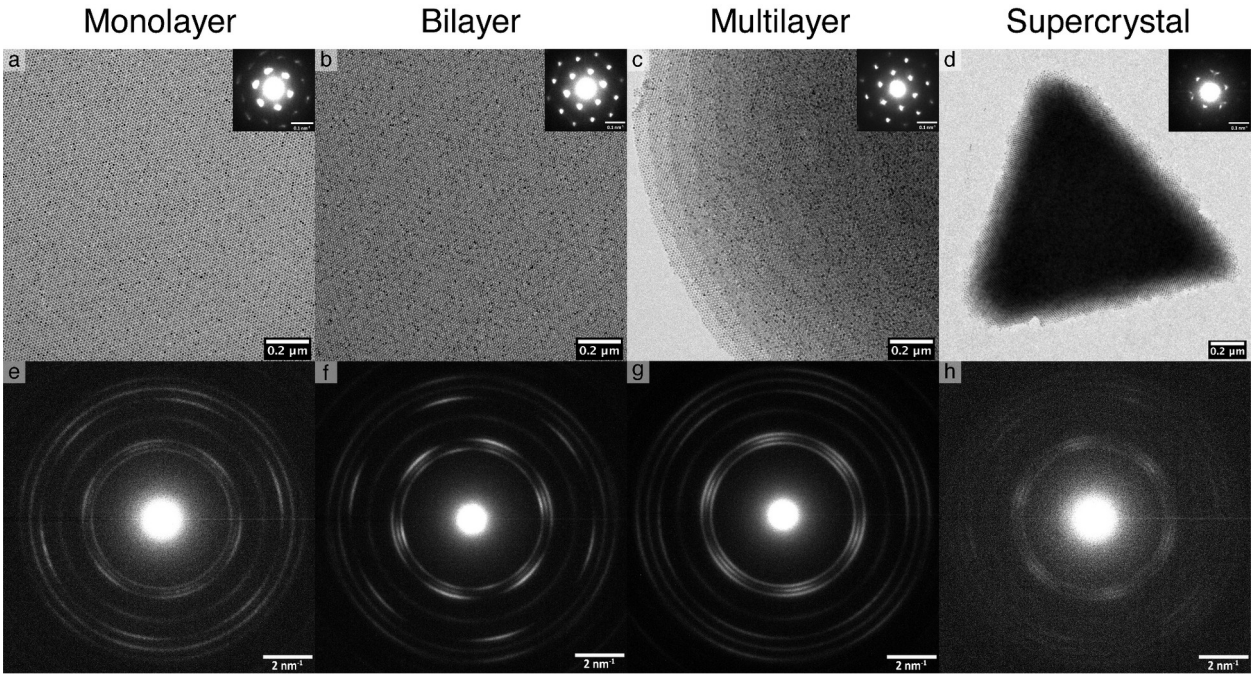


**Figure 5.** 2D and 3D superlattices made of oriented nanocrystals. (a-d) show large-area TEM images of the superlattice with their small-angle SAED in the inset indicating the hexagonal lattice. (e-h) are wide-angle SAED, which show the distinct orientations are maintained across a monolayer, bilayer, multilayer, and even a supercrystal.

## CONCLUSIONS

We showed that elliptically-faceted CdSe/CdS core/shell nanocrystals were not only able to form unexpectedly well-ordered translational superlattices, but they specifically formed an orientational glass phase in which only specific orientations were adopted by the nanocrystals. Despite having an apparently polydisperse ensemble, the nanocrystals were able to consistently form an orientational glass phase, even with different ligand coverage density, indicating that the shape is the main driving force in forming this phase. Our findings suggest that other possible

orientationally ordered phases, including nematic, smectic, and columnar phase, can form in self-assembled superlattices of lower-symmetry nanocrystals. In addition, our findings can be helpful for fundamental studies of orientational glass phases and their mechanism of formation.

METHODS

**Chemicals.**

Cadmium oxide (CdO, ≥ 99.99%), selenium (Se, 99.99%), trioctylphosphine oxide (TOPO, 99%), oleic acid (OA, 90%), oleylamine (OAm, 70%), 1-octadecene (ODE, 90%), 1-octanethiol (OctSH, ≥ 98.5%) were purchased from Sigma-Aldrich and used as received. Tri-n-octylphosphine (TOP, 99%, Strem). Octadecylphosphonic acid (ODPA, 99%, PCI Synthesis). Other chemicals used include diethylene glycol (DEG, 99%, Sigma-Aldrich), deuterated toluene (toluene-d8, 99%, Sigma-Aldrich), anhydrous toluene, isopropanol, and hexanes.

**Synthesis.**

**Elliptically-faceted CdSe/CdS core/shell Nanocrystals.**

Core nanocrystals were synthesized following a slightly modified version of previously published procedures[29,30]. 100 mg CdO, 471 mg ODPA, 5 g TOPO were placed in a 25 ml round-bottom flask and were degassed at 150 ºC for 30 minutes. The mixture was then heated to and maintained at 320 ºC under argon solution until it turned clear. At 320 ºC, 1.67 ml of TOP was injected in the solution and then the temperature was raised to 380 ºC. A pre-prepared 100 mg Se dissolved in 0.84 ml TOP was swiftly injected when temperature approached 380 ºC. Upon injection, CdSe nanocrystals were formed and were allowed to grow for 2 minutes to produce large and uniform cores, then cooled to 50 ºC before injecting 5 ml of toluene and transferring to an inert atmosphere. The nanocrystals were cleaned in an inert environment with successive precipitation and dissolution using hexanes and isopropanol, and were stored in 4ml hexane. Sizing and concentrations were determined by a previously reported empirical formula[31].

Shelled nanocrystals were synthesized by first degassing 3 ml ODE, 3 ml OAm and 100 nmol of CdSe cores in a 50 ml round-bottom flask at room temperature for 1 hr and at 120 ºC for 20 min. The solution was then heated to 310 ºC, and the injection of Cd and S precursor solutions in ODE started when the flask reached 230 ºC. The Cd precursor solution contained 4.74 ml of 0.20 mM $Cd(OA)_2$, and the S precursor contained 197.5 µl of OctSH in 4.54 ml ODE. The precursor solutions were injected at a rate of 2 ml/hr using a syringe pump. Upon completion of the precursor injections, the reaction was maintained at 310 ºC for 10 minutes, then cooled quickly to room temperature. Successive precipitation and dissolution using hexanes and isopropanol was done to clean the nanocrystals capped with OA and OAm before they were stored in 4 ml hexane in an inert atmosphere.

**Quasi-spherical CdSe/CdS core/shell Nanocrystals.**

Core nanocrystals were synthesized following similar previously published procedures[29]. Briefly, 120 mg CdO, 560 mg ODPA, 6 g TOPO were degassed under vacuum in a 50 mL round-bottom flask at 150 ºC for 1 hour. The mixture was then heated to 320 ºC under argon gas and maintained at 320 ºC until solution turned clear indicating formation of a complex. Upon completion of complex formation, 3 g of TOP was injected in the solution and then the temperature was raised to 360 ºC. A pre-prepared solution of 120 mg Se in 0.72 mL TOP was swiftly injected when temperature approached 360 ºC. Upon injection, CdSe nanocrystals were formed and were allowed to grow for 90 seconds to produce large, uniform cores. Solution was then rapidly cooled with compressed air to 120 ºC before injecting 10 mL of anhydrous toluene and transferring to an inert atmosphere. The nanocrystals were cleaned in an inert environment with successive precipitation and redispersion using acetone and hexane respectively and were

stored in 3ml of hexane. Size and concentrations were determined by a previously-reported empirical formula[32].

Shelled nanocrystals were synthesized by first degassing under vacuum 3 mL of ODE, 3 mL of OAm and 100 nmol of CdSe cores in a 25 mL round-bottom flask at 110 ºC for 30 mins. The solution was then heated to 310 ºC under Ar. When the temperature reached 240 ºC, injections of Cd and S precursor solutions in ODE started at a rate of 3 ml/hr using a syringe pump. The Cd precursor solution contained 2.96 mL of 0.20 mM Cd(OA)2 and the S precursor contained 86.6 mg of OctSH in 2.26 g of ODE. Upon completion of the precursor injections, the reaction was maintained at 310 ºC for 10 minutes, then cooled rapidly using compressed air to room temperature. Successive precipitation and redispersed using acetone and hexane respectively were done to clean the nanocrystals capped with OA and OAm before they were stored in 2 mL hexane in an inert atmosphere.

**Self-assembly of Nanocrystals Superlattice.**

The self-assembly was performed following a previously-published method[1]. Nanocrystal superlattices were formed on top of an immiscible liquid subphase at room temperature. Typically, the nanocrystal stock solution was diluted in hexane to achieve a proper concentration to form a monolayer superlattice. The solution was then drop-casted onto the surface of DEG in a Teflon well (1.5x1.5x1.5 $cm^3$). The well was then swiftly covered with double glass slides and vial on top to slow down the evaporation rate of hexane overnight. The superlattice was then formed and transferred onto a carbon-coated Cu TEM grid (400-mesh), which was then dried under vacuum for 1 hr at room temperature to remove residual DEG.

**TEM and Electron Diffraction Characterizations.**

Electron microscopy characterization followed a previously-published method[1]. The TEM, selected area electron diffraction (SAED) and HRTEM images were acquired on an FEI Tecnai T20 S-TWIN TEM operating at 200 kV with a LaB6 filament and equipped with a Gatan Rio 16IS camera with 4k resolution. Aberration corrected HRTEM and HAADF-STEM imaging were done on the TEAM 0.5 instrument at the Molecular Foundry at 300 kV. A 4k OneView detector was used to acquire aberration corrected HRTEM images. HAADF-STEM images were acquired with a 17.1 mrad convergence angle and about 70 pA of beam current.

**NMR.**

$^{1}$H NMR spectra were recorded with a Bruker Avance IV NEO spectrometer operating at 500 MHz and equipped with a 5 mm 1H/BB iProbe. The spectrometer runs on full automation using a SampleXpress autosampler which allows the collection of the samples with minimal human intervention. The nanocrystals were prepared by dispersing them in deuterated toluene (toluene-d8) right after they were precipitated by the anti-solvent in an inert environment. The data was then analyzed with Mnova software by Mestrelab Research.

**Translational Order Analysis.**

The image analysis was done following a previously-published method[5]. Briefly, the autocorrelation function was run on each TEM image using Gwyddion software, in which the image is adjusted by mean value subtraction, and the line profiles were extracted for different directions. The extracted data were then fitted with a two Gaussian function using a least-squares

method in Python. The Delaunay triangulation and Voronoi diagram were performed using freud software[26].

**Orientational Order Analysis.**

Further image analysis was performed in Python, using methods from the scipy and scikit-image libraries[33,34]. To begin, the TEM image was binarized using the Otsu thresholding method[35], and the center of mass of each nanocrystal was identified. Then, each nanocrystal was separated into its own image, where the FFT pattern is extracted. From the FFT, blob detection was used to calculate the lattice d-spacing and assign it to the corresponding lattice planes for the wurtzite CdSe/CdS system. Finally, the lattice planes were drawn on the crystal structure prepared with Vesta software and rotated based on the FFT pattern[36], and the orientation is identified using out-of-plane angle $\theta$ and the azimuthal angle $\varphi$ in a spherical coordinate with reference to the beam propagation direction.

.

ASSOCIATED CONTENT

The Supporting Information is available free of charge.

TEM image analysis of eccentricities as well as orientations of nanocrystals, $^{1}$H NMR characterization, translational autocorrelation function, and TEM of a square superlattice. (PDF)

AUTHOR INFORMATION

**Corresponding Author**

*To whom correspondence may be addressed: paul.alivisatos@berkeley.edu

**Present Addresses**

†A. Paul Alivisatos - Department of Chemistry and Pritzker School of Molecular Engineering, University of Chicago, Chicago, Illinois 60637, United States

**Author Contributions**

The manuscript was written through contributions of all authors. All authors have given approval to the final version of the manuscript.

**Funding Sources**

This work was supported by the U.S. Department of Energy, Office of Science, Office of Basic Energy Sciences, Materials Sciences and Engineering Division, under Contract No. DEAC02-05-CH11231 within the Inorganic/Organic Nanocomposites Program (KC3104).

**Notes**

The authors declare no competing financial interest.

ACKNOWLEDGMENT

This work was supported by the U.S. Department of Energy, Office of Science, Office of Basic Energy Sciences, Materials Sciences and Engineering Division, under Contract No. DEAC02-05-CH11231 within the Inorganic/Organic Nanocomposites Program (KC3104). The high-resolution TEM and STEM experiments were performed at the Molecular Foundry, Lawrence Berkeley National Laboratory, which is supported by the U.S. Department of Energy under contract no. DE-AC02-05CH11231.

REFERENCES


(1) Ye, X.; Zhu, C.; Ercius, P.; Raja, S. N.; He, B.; Jones, M. R.; Hauwiller, M. R.; Liu, Y.; Xu, T.; Alivisatos, A. P. Structural Diversity in Binary Superlattices Self-Assembled from Polymer-Grafted Nanocrystals. *Nat. Commun.* **2015**, *6*, 1-10.

(2) Coropceanu, I.; Boles, M. A.; Talapin, D. V. Systematic Mapping of Binary Nanocrystal Superlattices: The Role of Topology in Phase Selection. *J. Am. Chem. Soc.* **2019**, *141*, 5728–5740.

(3) Rainò, G.; Becker, M. A.; Bodnarchuk, M. I.; Mahrt, R. F.; Kovalenko, M. V.; Stöferle, T. Superfluorescence from Lead Halide Perovskite Quantum Dot Superlattices. *Nature* **2018**, *563*, 671–675.

(4) Boles, M. A.; Engel, M.; Talapin, D. V. Self-Assembly of Colloidal Nanocrystals: From Intricate Structures to Functional Materials. *Chem. Rev.* **2016**, *116*, 11220–11289.

(5) Pichler, S.; Bodnarchuk, M. I.; Kovalenko, M. V.; Yarema, M.; Springholz, G.; Talapin, D. V.; Heiss, W. Evaluation of Ordering in Single-Component and Binary Nanocrystal Superlattices by Analysis of Their Autocorrelation Functions. *ACS Nano* **2011**, *5*, 1703–1712.

(6) Donev, A.; Stillinger, F. H.; Chaikin, P. M.; Torquato, S. Unusually Dense Crystal Packings of Ellipsoids. *Phys. Rev. Lett.* **2004**, *92*, 1–4.

(7) Donev, A.; Cisse, I.; Sachs, D.; Torquato, S.; Chaikin, P. M. Improving the Density of Jammed Disordered Packings Using Ellipsoids. *Science* **2004**, *303*, 990–993.

(8) Damasceno, P. F.; Engel, M.; Glotzer, S. C. Predictive Self-Assembly of Polyhedra into

Complex Structures. *Science* **2012**, *337*, 453–457.

(9) Zhu, H.; Fan, Z.; Yu, L.; Wilson, M. A.; Nagaoka, Y.; Eggert, D.; Cao, C.; Liu, Y.; Wei, Z.; Wang, X.; He, J.; Zhao, J.; Li, R.; Wang, Z.; Grünwald, M.; Chen, O. Controlling Nanoparticle Orientations in the Self-Assembly of Patchy Quantum Dot-Gold Heterostructural Nanocrystals. *J. Am. Chem. Soc.* **2019**, *141*, 6013–6021.

(10) Zaitseva, N.; Dai, Z. R.; Leon, F. R.; Krol, D. Optical Properties of CdSe Superlattices. *J. Am. Chem. Soc.* **2005**, *127*, 10221-10226.

(11) Simon, P.; Rosseeva, E.; Baburin, I. A.; Liebscher, L.; Hickey, S. G.; Cardoso-Gil, R.; Eychmüller, A.; Kniep, R.; Carrillo-Cabrera, W. PbS-Organic Mesocrystals: The Relationship between Nanocrystal Orientation and Superlattice Array. *Angew. Chem. Int. Ed.* **2012**, *51*, 10776–10781.

(12) Choi, J. J.; Bealing, C. R.; Bian, K.; Hughes, K. J.; Zhang, W.; Smilgies, D. M.; Hennig, R. G.; Engstrom, J. R.; Hanrath, T. Controlling Nanocrystal Superlattice Symmetry and Shape-Anisotropic Interactions through Variable Ligand Surface Coverage. *J. Am. Chem. Soc.* **2011**, *133*, 3131–3138.

(13) DaSilva, J. C.; Smeaton, M. A.; Dunbar, T. A.; Xu, Y.; Balazs, D. M.; Kourkoutis, L. F.; Hanrath, T. Mechanistic Insights into Superlattice Transformation at a Single Nanocrystal Level Using Nanobeam Electron Diffraction. *Nano Lett.* **2020**, *20*, 5267–5274.

(14) Choi, J. J.; Bian, K.; Baumgardner, W. J.; Smilgies, D. M.; Hanrath, T. Interface-Induced Nucleation, Orientational Alignment and Symmetry Transformations in Nanocube Superlattices. *Nano Lett.* **2012**, *12*, 4791–4798.

(15) Lee, Y. H.; Shi, W.; Yang, Y.; Kao, Y. C.; Lee, H. K.; Chu, R.; Pang, Y. L.; Lay, C. L.;

Li, S.; Ling, X. Y. Modulating Orientational Order to Organize Polyhedral Nanoparticles into Plastic Crystals and Uniform Metacrystals. *Angew. Chem. Int. Ed.* **2020**, *59*, 21183–21189.

(16) Wu, Y.; Li, S.; Gogotsi, N.; Zhao, T.; Fleury, B.; Kagan, C. R.; Murray, C. B.; Baxter, J. B. Directional Carrier Transfer in Strongly Coupled Binary Nanocrystal Superlattice Films Formed by Assembly and in Situ Ligand Exchange at a Liquid-Air Interface. *J. Phys. Chem. C* **2017**, *121*, 4146–4157.

(17) Weidman, M. C.; Smilgies, D. M.; Tisdale, W. A. Kinetics of the Self-Assembly of Nanocrystal Superlattices Measured by Real-Time in Situ X-Ray Scattering. *Nat. Mater.* **2016**, *15*, 775–781.

(18) Folmer, J. C. W.; Withers, R. L.; Welberry, T. R.; Martin, J. D. Coupled Orientational and Displacive Degrees of Freedom in the High-Temperature Plastic Phase of the Carbon Tetrabromide α-CBr4. *Phys. Rev. B* **2008**, *77*, 1-10.

(19) Zaluzhnyy, I. A.; Kurta, R. P.; André, A.; Gorobtsov, O. Y.; Rose, M.; Skopintsev, P.; Besedin, I.; Zozulya, A. V.; Sprung, M.; Schreiber, F.; Vartanyants, I. A.; Scheele, M. Quantifying Angular Correlations between the Atomic Lattice and the Superlattice of Nanocrystals Assembled with Directional Linking. *Nano Lett.* **2017**, *17*, 3511–3517.

(20) Tan, R.; Yuan, Y.; Nagaoka, Y.; Eggert, D.; Wang, X.; Thota, S.; Guo, P.; Yang, H.; Zhao, J.; Chen, O. Monodisperse Hexagonal Pyramidal and Bipyramidal Wurtzite CdSe-CdS Core-Shell Nanocrystals. *Chem. Mater.* **2017**, *29*, 4097–4108.

(21) Cui, J.; Pan, Y. E.; Koley, S.; Shamalia, D.; Waiskopf, N.; Remennik, S.; Popov, I.; Oded, M.; Banin, U. Colloidal Quantum Dot Molecules Manifesting Quantum Coupling at Room

Temperature. *Nat. Commun.* **2019**, *10*, 1-10.

(22) Mukharamova, N.; Lapkin, D.; Zaluzhnyy, I. A.; André, A.; Lazarev, S.; Kim, Y. Y.; Sprung, M.; Kurta, R. P.; Schreiber, F.; Vartanyants, I. A.; Scheele, M. Revealing Grain Boundaries and Defect Formation in Nanocrystal Superlattices by Nanodiffraction. *Small* **2019**, *15*, 1-8.

(23) Shintani, H.; Tanaka, H. Frustration on the Way to Crystallization in Glass. *Nat. Phys.* **2006**, *2*, 200–206.

(24) Takae, K.; Onuki, A. Orientational Glass in Mixtures of Elliptic and Circular Particles: Structural Heterogeneities, Rotational Dynamics, and Rheology. *Phys. Rev. E* **2014**, *89*, 1-14.

(25) Karas, A. S.; Dshemuchadse, J.; Van Anders, G.; Glotzer, S. C. Phase Behavior and Design Rules for Plastic Colloidal Crystals of Hard Polyhedra: Via Consideration of Directional Entropic Forces. *Soft Matter* **2019**, *15*, 5380–5389.

(26) Ramasubramani, V.; Dice, B. D.; Harper, E. S.; Spellings, M. P.; Anderson, J. A.; Glotzer, S. C. Freud: A Software Suite for High Throughput Analysis of Particle Simulation Data. *Comput. Phys. Commun.* **2020**, *254*.

(27) McCray, A. R. C.; Savitzky, B. H.; Whitham, K.; Hanrath, T.; Kourkoutis, L. F. Orientational Disorder in Epitaxially Connected Quantum Dot Solids. *ACS Nano* **2019**, *13*, 11460–11468.

(28) Agarwal, U.; Escobedo, F. A. Mesophase Behaviour of Polyhedral Particles. *Nat. Mater.* **2011**, *10*, 230–235.

(29) Chen, O.; Zhao, J.; Chauhan, V. P.; Cui, J.; Wong, C.; Harris, D. K.; Wei, H.; Han, H.-S.;

Fukumura, D.; Jain, R. K.; Bawendi, M. G. Compact High-Quality CdSe-CdS Core-Shell Nanocrystals with Narrow Emission Linewidths and Suppressed Blinking. *Nat. Mater.* **2013**, *12*, 445–451.

(30) Olshansky, J. H.; Ding, T. X.; Lee, Y. V.; Leone, S. R.; Alivisatos, A. P. Hole Transfer from Photoexcited Quantum Dots: The Relationship between Driving Force and Rate. *J. Am. Chem. Soc.* **2015**, *137*, 15567–15575.

(31) Jasieniak, J.; Smith, L.; Embden, J. Van; Mulvaney, P.; Califano, M. Re-Examination of the Size Dependent Absorption Properties of CdSe Quantum Dots. *J. Phys. Chem. C* **2009**, *113*, 19468–19474.

(32) Yu, W. W.; Qu, L.; Guo, W.; Peng, X. Experimental Determination of the Extinction Coefficient of CdTe, CdSe and CdS Nanocrystals. *Chem. Mater.* **2003**, *15*, 2854-2860.

(33) Virtanen, P.; Gommers, R.; Oliphant, T. E.; Haberland, M.; Reddy, T.; Cournapeau, D.; Burovski, E.; Peterson, P.; Weckesser, W.; Bright, J.; van der Walt, S. J.; Brett, M.; Wilson, J.; Millman, K. J.; Mayorov, N.; Nelson, A. R. J.; Jones, E.; Kern, R.; Larson, E.; Carey, C. J.; Polat, İ.; Feng, Y.; Moore, E. W.; VanderPlas, J.; Laxalde, D.; Perktold, J.; Cimrman, R.; Henriksen, I.; Quintero, E. A.; Harris, C. R.; Archibald, A. M.; Ribeiro, A. H.; Pedregosa, F.; van Mulbregt, P.; and SciPy 1.0 Contributors. SciPy 1.0: Fundamental Algorithms for Scientific Computing in Python. *Nat. Methods* **2020**, *17*, 261–272.

(34) Van Der Walt, S.; Schönberger, J. L.; Nunez-Iglesias, J.; Boulogne, F.; Warner, J. D.; Yager, N.; Gouillart, E.; Yu, T.; and the scikit-image contributors. Scikit-Image: Image Processing in Python. *PeerJ* **2014**, *2:e453*, 1–18.

(35) Otsu, N. A Threshold Selection Method from Gray-Level Histograms. *IEEE Trans. Syst.*

*Man. Cybern.* **1979**, *SMC-9*, 62–66.

(36) Momma, K.; Izumi, F. VESTA 3 for Three-Dimensional Visualization of Crystal, Volumetric and Morphology Data. *J. Appl. Crystallogr.* **2011**, *44*, 1272–1276.

TOC